

## REVIEW

### Eastern North Pacific Hurricane Season of 2009

TODD B. KIMBERLAIN AND MICHAEL J. BRENNAN

*NOAA/NWS/NCEP National Hurricane Center, Miami, Florida*

(Manuscript received 10 May 2010, in final form 10 September 2010)

#### ABSTRACT

The 2009 eastern North Pacific hurricane season had near normal activity, with a total of 17 named storms, of which seven became hurricanes and four became major hurricanes. One hurricane and one tropical storm made landfall in Mexico, directly causing four deaths in that country along with moderate to severe property damage. Another cyclone that remained offshore caused an additional direct death in Mexico. On average, the National Hurricane Center track forecasts in the eastern North Pacific for 2009 were quite skillful.

#### 1. Introduction

After two quieter-than-average hurricane seasons, tropical cyclone (TC) activity in the eastern North Pacific basin<sup>1</sup> during 2009 (Fig. 1; Table 1) was near normal. A total of 17 tropical storms developed, of which seven became hurricanes and four became major hurricanes [maximum 1-min 10-m winds greater than 96 kt ( $1 \text{ kt} = 0.5144 \text{ m s}^{-1}$ ), corresponding to category 3 or greater on the Saffir–Simpson Hurricane Wind Scale (Saffir 1973; Simpson 1974; Schott et al. 2010)]. In addition, two tropical depressions formed that did not strengthen into tropical storms, and another tropical depression formed over the far western part of the basin and reached tropical storm strength in the central North Pacific basin (west of  $140^{\circ}\text{W}$ ). Although the number of hurricanes was below the 1971–2008 average of 9, the seasonal numbers of named storms and major hurricanes were close to the long-term averages of 15 and 4, respectively. Hurricane Rick became the second-strongest hurricane observed in the eastern North Pacific since reliable records began in 1971; only Linda of 1997 was stronger. Rick was also the strongest hurricane ever observed in the basin during the month of October. Hurricanes

Jimena and Rick made landfall in Mexico this season, the latter as a tropical storm. Hurricane Andres also affected Mexico as it passed offshore of that nation's southern coast. Tropical Storm Patricia briefly threatened the southern tip of the Baja California peninsula before weakening.

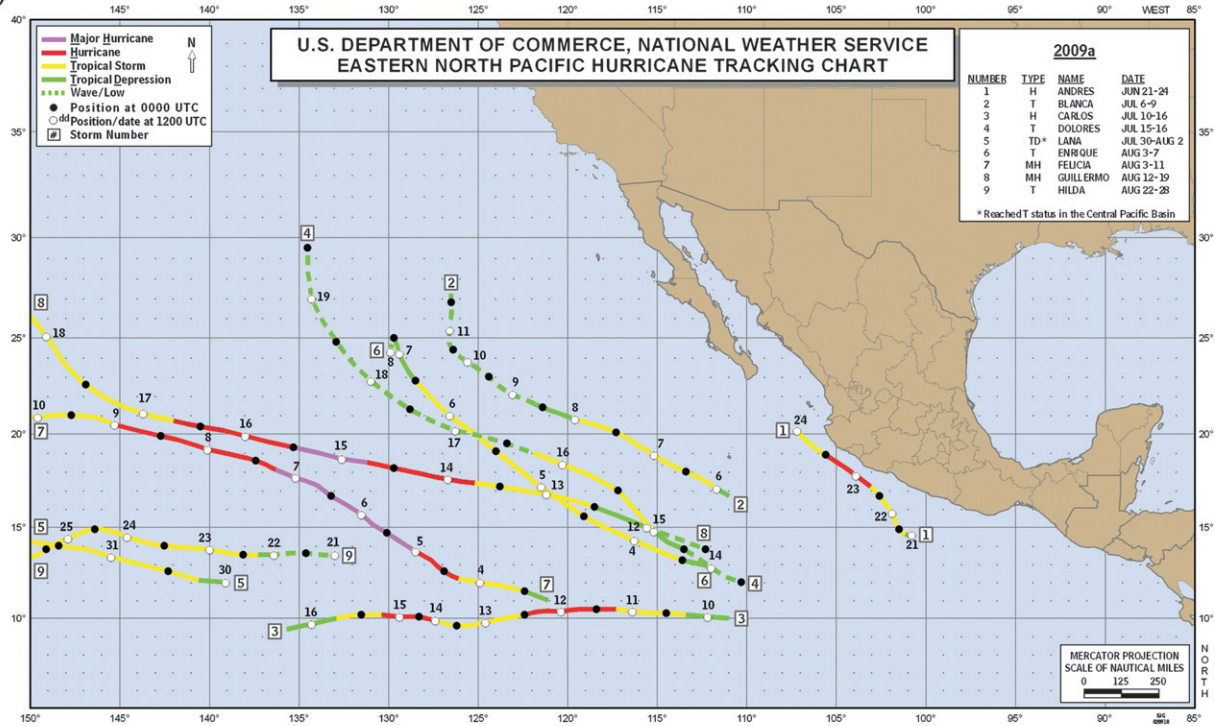
A parameter routinely used to gauge the overall activity of a season is the “accumulated cyclone energy” (ACE) index (Bell et al. 2000). The ACE index, which accounts for both the intensity and duration of the season's storms, is calculated by summing the squares of the maximum sustained wind speed at 6-h intervals for all (sub)tropical storms and hurricanes. The ACE for the 2009 season was  $102 \times 10^4 \text{ kt}^2$  or about 93% of the long-term (1971–2005) median value of  $109 \times 10^4 \text{ kt}^2$ , which places 2009 in the near-average (middle) historical tercile for activity. Since 1995, TC activity in the eastern North Pacific has generally remained below the long-term median except during seasons when an El Niño was occurring.

During 2009, above-normal sea surface temperatures, a well-known characteristic of El Niño events, were observed in the tropical and subtropical eastern Pacific (Fig. 2), and these conditions may have contributed to the increased activity in the basin. Also of note is that 13 of the 17 named storms in 2009 formed west of  $110^{\circ}\text{W}$ , the most since 1994 (another El Niño year). Composite data from the National Centers for Environmental Prediction (NCEP)–National Center for Atmospheric Research (NCAR) reanalysis (Kalnay et al. 1996) suggest that the westward displacement of genesis locations may have

<sup>1</sup> As defined here, the eastern North Pacific basin extends from the west coast of North America to  $140^{\circ}\text{W}$ .

*Corresponding author address:* Todd B. Kimberlain, National Hurricane Center, 11691 SW 17th Street, Miami, FL 33165.  
E-mail: todd.kimberlain@noaa.gov

(a)



(b)

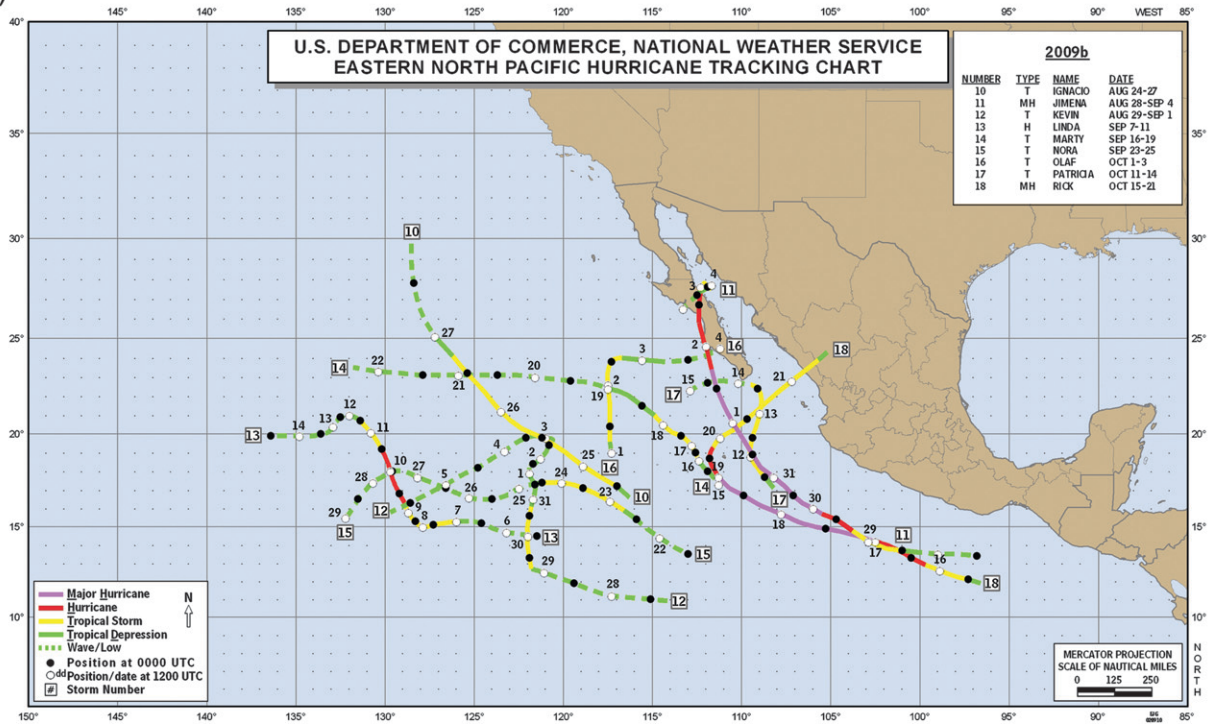


FIG. 1. (Continued)

(c)

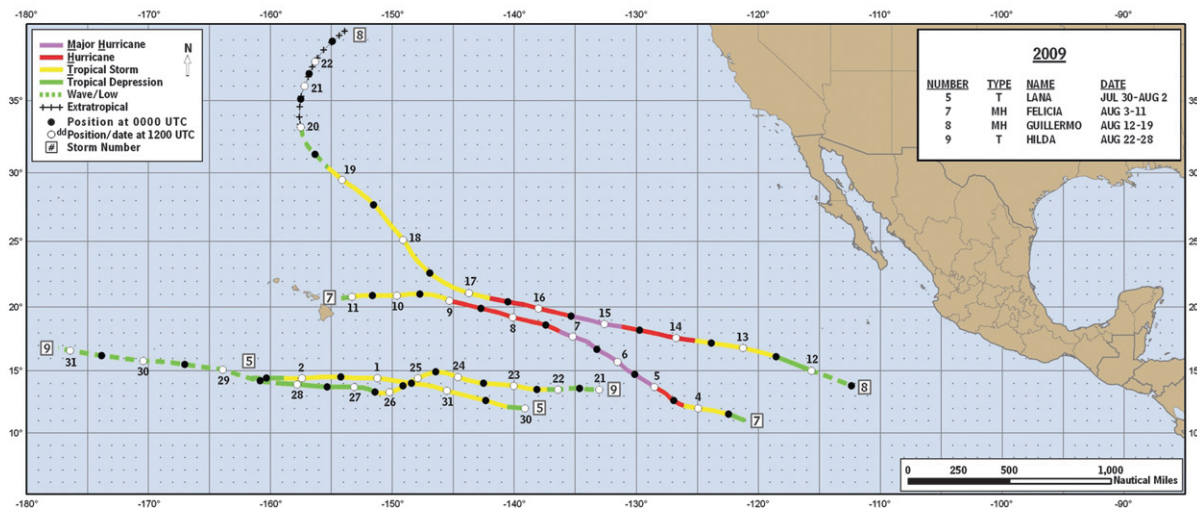


FIG. 1. (a) Tracks of the first eight tropical storms and hurricanes in the eastern North Pacific basin in 2009 (including remnant low stage) and Tropical Storm Lana, which was named in the central North Pacific basin. (b) Tracks of the final nine tropical storms and hurricanes in the eastern North Pacific basin in 2009, including remnant low stage. (c) Tracks of the four tropical cyclones that crossed into the central North Pacific basin (west of 140°W) in 2009, including remnant low and extratropical stages.

been associated with the large-scale negative 200-hPa velocity potential anomalies (associated with divergence) (Fig. 3) that extended westward from 120°W to at least the International Date Line. The increased activity in the western portion of the basin is consistent with the work of Collins (2007), who found that seasonal TC activity west of 116°W is closely tied to El Niño–Southern Oscillation (ENSO). The westward displacement of TC activity contributed to a large number of weak and short-lived systems (eight had life spans of three days or less), since many TCs formed closer to cooler waters and quickly encountered increased vertical wind shear (Fig. 4) in the western part of the basin (west of 120°W and north of 10°N).

The 2009 season started unusually late, with Andres forming on 21 June, more than three weeks after the 29 May median date for the first named storm. The month of August was unusually active, with seven named storms forming. This marked the formation of the most named storms in any month since 1985 and the most forming in the month of August since 1968, when eight developed. Also, August marked the first time since 1998 that three major hurricanes formed in any single month in the basin. The season ended with the dissipation of Rick on 21 October, very close to the median end date.

The second section focuses on data used to analyze the season’s tropical cyclones. Section 3 provides individual narratives of tropical cyclone life cycles for all named storms; section 4 describes unnamed tropical depressions. The final section discusses and critiques the verification of National Hurricane Center (NHC) track and intensity forecasts for the 2009 season.

## 2. Data

The individual cyclone summaries that follow in section 3 are based on poststorm meteorological analyses conducted at the NHC utilizing a wide variety of data described below. These analyses result in the creation of a “best-track” database for each cyclone, consisting of 6-hourly representative estimates of the cyclone’s center position, maximum sustained (1-min average) surface (10-m) wind, minimum sea level pressure, and the maximum extent of 34-, 50-, and 64-kt winds in each of the four quadrants around the cyclone’s center. The life cycle of each cyclone (as indicated by the dates given in Table 1) includes the tropical depression stage but does not include remnant low or extratropical stages. The tracks and basic statistics for the season’s tropical storms and hurricanes are given in Fig. 1 and Table 1 (see <http://www.nhc.noaa.gov/pastall.shtml> for more complete track data).<sup>2</sup>

Observations of eastern North Pacific tropical cyclones are almost exclusively obtained from satellites, with the National Oceanic and Atmospheric Administration (NOAA) Geostationary Operational Environmental Satellites (GOES) serving as the primary platform. GOES-East and GOES-West provide the visible and

<sup>2</sup> The Web site contains tabulations of the 6-hourly best track positions and intensities from the NHC’s Tropical Cyclone Reports. These reports contain storm information omitted here due to limitations of space, including additional surface observations and a forecast and warning critique.

TABLE 1. Eastern North Pacific tropical storms and hurricanes of 2009.

Name	Class*	Dates**	Max 1-min wind (kt)	Min sea level pressure (mb)	Direct deaths
Andres	H	21–24 Jun	70	984	1
Blanca	TS	6–9 Jul	45	998	
Carlos	H	10–16 Jul	90	971	
Dolores	TS	15–16 Jul	50	997	
Enrique	TS	3–7 Aug	55	994	
Felicia	MH	3–11 Aug	125	935	
Guillermo	MH	12–19 Aug	110	954	
Hilda	TS	22–28 Aug	55	995	
Ignacio	TS	24–27 Aug	45	999	
Jimena	MH	28 Aug–4 Sep	135	931	1
Kevin	TS	29 Aug–1 Sep	45	1000	
Linda	H	7–11 Sep	70	985	
Marty	TS	16–19 Sep	40	1002	
Nora	TS	23–25 Sep	50	997	
Olaf	TS	1–3 Oct	40	996	
Patricia	TS	11–14 Oct	50	996	
Rick	MH	15–21 Oct	155	906	2

\* TS = tropical storm, wind speed 34–63 kt ( $17\text{--}32\text{ m s}^{-1}$ ); H = hurricane, wind speed 64 kt ( $33\text{ m s}^{-1}$ ) or higher; MH, major hurricane, hurricane with maximum winds 96 kt ( $49\text{ m s}^{-1}$ ) or higher.

\*\* Dates are based on UTC and include the tropical depression stage but exclude the remnant low and extratropical stages.

infrared imagery that serves as input for intensity estimates based on the Dvorak (1984) classification technique. Subjective Dvorak intensity estimates utilized by NHC are performed by NHC's Tropical Analysis and Forecast Branch (TAFB) and the Satellite Analysis Branch (SAB) in Camp Springs, Maryland. The advanced Dvorak technique (ADT; Olander and Velden 2007) is an objective method that also provides satellite intensity estimates of TCs using geostationary imagery.

Geostationary imagery is occasionally supplemented by passive microwave imagery from NOAA polar-orbiting satellites, Defense Meteorological Satellite Program (DMSP) satellites, the U.S. Navy's WindSat, and National Aeronautics and Space Administration (NASA) satellites that include the Tropical Rainfall Measuring Mission (TRMM) and *Aqua* instruments. Such imagery is useful for tracking TCs and assessing their structure (Hawkins et al. 2001). Ocean surface vector wind retrievals from the NASA Quick Scatterometer (QuikSCAT)<sup>3</sup> and the European Space Agency's Advanced Scatterometer (ASCAT) were also useful for analysis of the location, intensity, and outer wind radii of a TC (e.g., Brennan et al. 2009). In addition, these data can be helpful in resolving whether an incipient TC has acquired a closed surface circulation. Finally, information about the thermal structure of cyclone cores is provided by the Advanced Microwave Sounder Unit (AMSU; Demuth et al. 2006; Brueske and Velden 2003). Intensity estimates derived

from these AMSU data can sometimes be superior to Dvorak classifications (Herndon et al. 2004).

Ships occasionally provide important in situ observations. For systems posing a threat to land, direct measurements from reconnaissance aircraft are often available. The 53rd Weather Reconnaissance Squadron of the United States Air Force Reserve Command (AFRC) flew five reconnaissance missions into eastern North Pacific tropical cyclones during 2009: one in Andres, two in Jimena, and two in Rick. These missions provided flight-level data as well as surface wind estimates from the Stepped-Frequency Microwave Radiometer (SFMR; Ulhorn and Black 2003). Land-based radars from the Meteorological Service of Mexico were also useful for monitoring TCs during 2009.

For a more complete description of the observational platforms used in TC analysis at NHC, see Rappaport et al. (2009).

### 3. Individual storm summaries

#### a. Hurricane Andres, 21–24 June

Andres originated from a tropical wave that entered the eastern North Pacific on 16 June. Convective activity associated with the wave gradually increased over the next few days as the wave moved slowly westward, and an area of low pressure formed along the wave axis on 20 June about 150 n mi south-southeast of Acapulco, Mexico. Associated convective activity became better organized early the next day, and by 1200 UTC a tropical depression formed.

<sup>3</sup> The QuikSCAT mission ended in November 2009 when the instrument became inoperative.

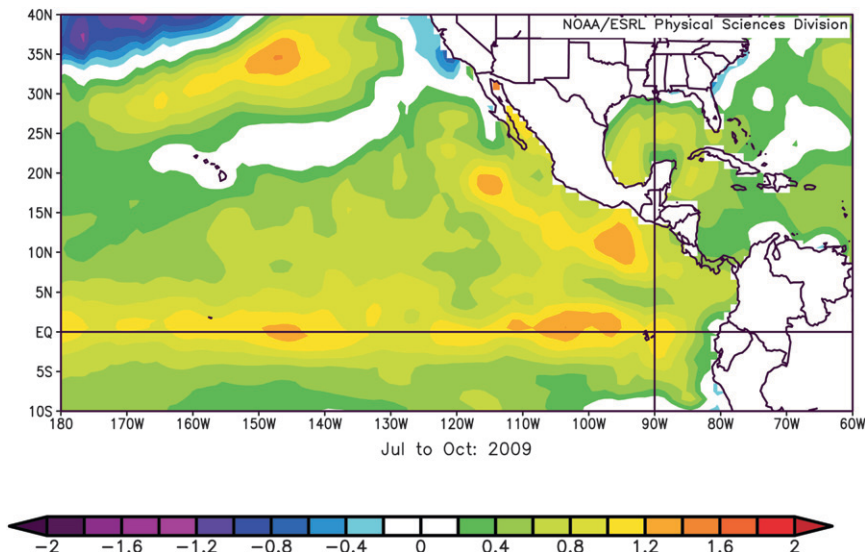


FIG. 2. Composite sea surface temperature (SST) anomaly (shaded every 0.2°C) for July to October 2009 from the NOAA Optimum Interpolation SST analysis. Anomaly computed from the 1971–2000 climatology. Image provided by the NOAA/ESRL Physical Sciences Division, Boulder, Colorado, from their Web site (<http://www.esrl.noaa.gov/psd>).

The tropical cyclone moved westward and strengthened into a tropical storm 6 h after genesis. Andres turned northwestward around the southwestern periphery of a midtropospheric ridge and continued on that heading for nearly the remainder of its existence. Over warm waters and in light vertical wind shear, Andres steadily intensified during the next 36 h. The cyclone attained hurricane strength just after 0000 UTC 23 June and reached an estimated peak intensity of 70 kt around 0600 UTC that day, while located about 70 n mi southwest of Lázaro Cárdenas, Mexico.

As Andres moved nearly parallel to the southwestern coast of Mexico, northeasterly shear increased, which initiated weakening. The center of Andres passed within about 50 n mi of the southwestern coast of Mexico, and the hurricane weakened to a tropical storm around 0000 UTC 24 June. Andres may have produced tropical-storm-force winds along a portion of the southwestern coast of Mexico, although no such winds were reported. The highest sustained wind recorded at a land-based station was 30 kt with a gust to 40 kt at Manzanillo, Mexico, late on 23 June. Shortly after 0000 UTC 24 June, cooler waters, a more stable air mass, and continued northeasterly shear led to a rapid weakening of the cyclone. Andres weakened to a tropical depression by 1200 UTC while centered about 85 n mi west of Cabo Corrientes, Mexico, and then turned northward and became an open trough of low pressure by 1800 UTC.

An Air Force reconnaissance aircraft reached Andres around 1800 UTC 23 June and the SFMR instrument

measured winds of 63 and 67 kt to the southeast and west of the center, respectively. In addition, two dropwindsondes released east of the center measured instantaneous surface winds of 65 and 66 kt. These data indicate that Andres’ maximum winds at that time were at least 65 kt, although its satellite appearance had been more impressive before the aircraft arrived. Thus the peak intensity of Andres is assumed to have been slightly higher 6–12 h earlier.

Andres was responsible for one death in Mexico: a man drowned while fishing in rough seas near Tépican de Galeana, between Acapulco and Zihuatanejo. Press reports indicate that damage along the southwestern coast

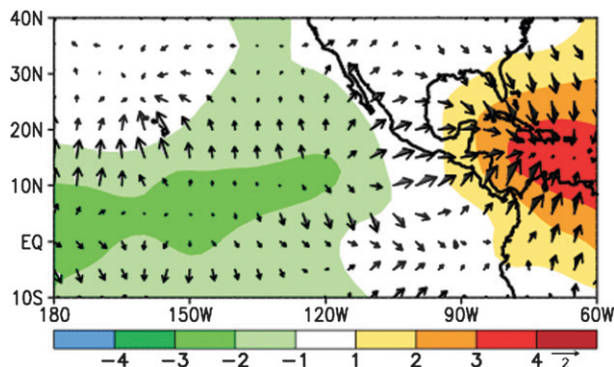


FIG. 3. Composite of July–September 2009 200-hPa velocity potential anomaly (shaded,  $m^2 s^{-1}$ ) and divergent wind anomaly (arrows,  $m s^{-1}$ , scale given in lower right) from the NCEP–NCAR reanalysis.

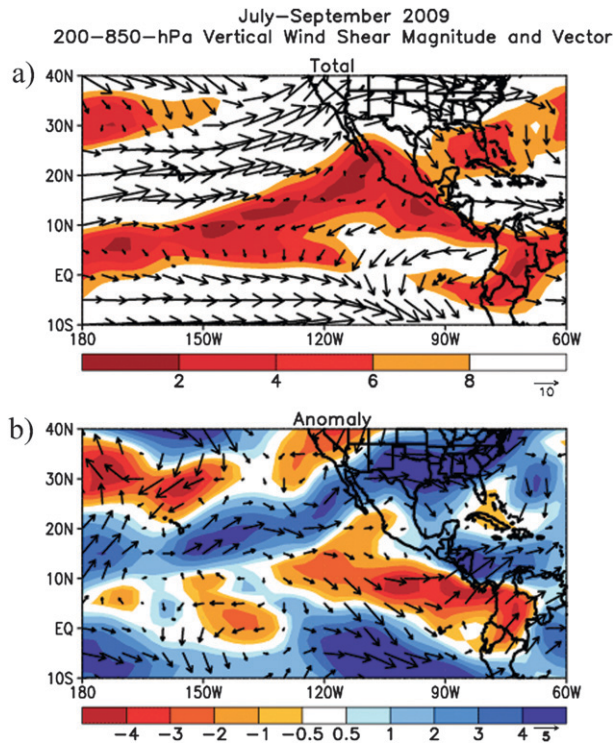


FIG. 4. (a) Composite mean of July–September 2009 200–850-hPa vertical wind shear magnitude (shaded,  $\text{m s}^{-1}$ ) and vector (scale given in lower right) from the NCEP–NCAR reanalysis. (b) July–September 2009 200–850-hPa vertical wind shear anomaly magnitude (shaded,  $\text{m s}^{-1}$ ) and vector (scale given in lower right) from the NCEP–NCAR reanalysis. Anomaly computed from the 1971–2000 climatology.

of Mexico was minimal. Heavy rains from Andres and its precursor disturbance flooded homes in a portion of Acapulco, which resulted in the evacuation of about 200 people.

#### b. Tropical Storm Blanca, 6–9 July

Blanca formed from a tropical wave that moved across the west coast of Africa on 19 June and entered the eastern North Pacific on 29 June. On 4 July, deep convection became consolidated in association with a broad surface low a few hundred nautical miles to the south of Manzanillo. Additional slow development occurred over the next two days, and the system became a tropical depression around 0600 UTC 6 July while centered about 380 n mi south of Cabo San Lucas, Mexico.

The flow to the south of a broad midlevel ridge steered the cyclone on a west-northwestward course at about 10 kt throughout its lifetime. About 6 h after genesis, the system strengthened into a tropical storm, and Blanca is estimated to have reached its maximum intensity of 45 kt around 0000 UTC 7 July. Later that day, Blanca moved over an area of sea surface temperatures below

$27^{\circ}\text{C}$  and began to gradually weaken as deep convection associated with the system became intermittent. Blanca weakened to a tropical depression by 1200 UTC 8 July and degenerated into a remnant low pressure area by 0600 UTC 9 July, about 690 n mi west of Cabo San Lucas. The circulation remained well defined as it turned northward from 10 to 11 July and then dissipated over the open waters of the subtropical eastern North Pacific by 0600 UTC 12 July.

#### c. Hurricane Carlos, 10–16 July

The origin of Carlos can be traced to a tropical wave that moved across the west coast of Africa on 25 June. The wave moved westward across the tropical Atlantic and Caribbean Sea with sporadic convection and reached the eastern North Pacific on 4 July. Convection associated with the wave began to increase and show signs of organization on 8 July, and it is estimated that a tropical depression formed around 0600 UTC 10 July about 780 n mi south of the southern tip of Baja California.

The depression continued moving westward along  $10^{\circ}\text{N}$  over warm waters in an environment of low vertical wind shear and became a tropical storm around 1800 UTC 10 July. Steady intensification followed, and Carlos became a hurricane around 1800 UTC 11 July. The relatively small cyclone achieved an intensity of 75 kt and developed an eye by 0000 UTC 12 July. After maintaining this intensity for about 12 h, the eye became obscured in geostationary imagery, and the cloud pattern became disorganized. Carlos weakened quickly and its intensity decreased to 45 kt by 0000 UTC 13 July. At that point, a new round of intensification began. Carlos redeveloped a small but well-defined eye in geostationary imagery, and the cyclone reached an estimated peak intensity of 90 kt at 0000 UTC 15 July. The peak intensity estimate of Carlos is more uncertain than normal since it was based on Dvorak estimates for an unusually small hurricane, for which there are not many cases in the technique's developmental sample (Erickson 1972; Velden et al. 2006).

Carlos encountered strong vertical wind shear as it approached  $130^{\circ}\text{W}$  on 15 July, resulting in an abrupt deterioration of the cloud pattern. The cyclone weakened rapidly from its peak intensity to a tropical depression in about a day. By 0000 UTC 17 July, the circulation of Carlos dissipated about 1900 n mi west-southwest of the southern tip of Baja California.

#### d. Tropical Storm Dolores, 15–16 July

Dolores formed from a tropical wave that moved across the coast of Africa on 1 July and reached the eastern North Pacific on 8 July. Once the wave slowed down on its westward course, a large, poorly defined low pressure area developed several hundred miles south of Acapulco

on 11 July. The circulation became better defined and the associated convection became better organized on 14 July as the system moved west-northwestward. It is estimated that a tropical depression formed around 0000 UTC 15 July about 605 n mi west-southwest of Manzanillo.

The cyclone moved generally northwestward on the southwestern side of a midlevel ridge over northern Mexico and the adjacent Pacific Ocean. Although the depression was located in an environment of moderate southwesterly vertical wind shear, it strengthened to a tropical storm about 12 h after genesis. Dolores reached a peak intensity of 50 kt around 0000 UTC 16 July about 540 n mi southwest of the southern tip of Baja California. The associated convection dissipated shortly afterward, and Dolores became a gale-force nontropical low around 1800 UTC 16 July; its peak winds fell below gale force about 6 h later. The remnant low of Dolores moved northwestward until 19 July and then turned northward before dissipating the next day about 865 n mi west-southwest of Los Angeles, California.

#### e. Tropical Storm Enrique, 3–7 August

Enrique formed from a tropical wave that moved across the west coast of Africa on 21 July. Deep convection developed near the wave as it crossed Central America on 30 July, but the convection remained disorganized for several days. By 3 August, deep convection increased further, and a tropical depression formed around 1800 UTC that day about 580 n mi southwest of Manzanillo. The depression became a tropical storm 6 h later and quickly reached its peak strength before the low-level center became exposed to the northwest of the deep convection later on 4 August.

Enrique moved west-northwestward and then north-northwestward over the next few days, with steering provided by the subtropical midlevel ridge to its north and the circulation of Hurricane Felicia to its west. The cyclone reached sea surface temperatures below 27°C on 5 August, and the cooler waters combined with northerly shear to cause the cyclone to slowly weaken. Enrique weakened to a tropical depression around 0000 UTC 7 August about 790 n mi west-southwest of Punta Eugenia, Mexico, and degenerated into a remnant low by 0000 UTC 8 August. The low then began moving slowly south-southwestward under the influence of the low-level flow and dissipated about 18 h later.

#### f. Hurricane Felicia, 3–11 August

Felicia's genesis can be traced to a tropical wave that was first detected in satellite imagery over the tropical Atlantic on 23 July. The wave began to develop convection after it moved into the eastern North Pacific on 29 July. After the wave passed 110°W on 1 August, deep

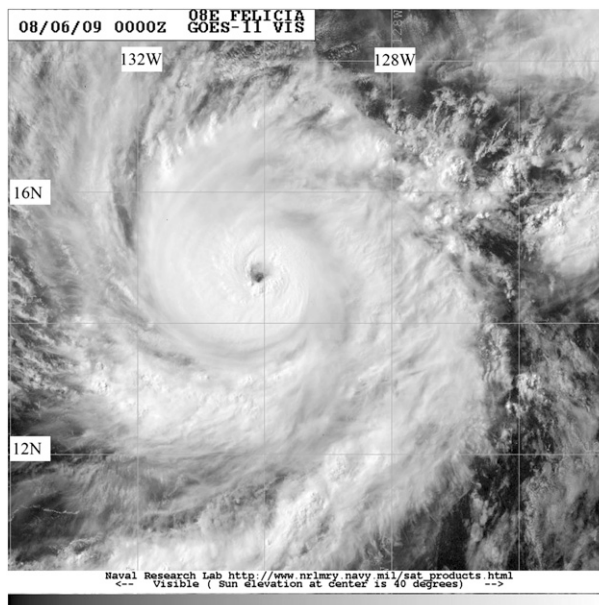


FIG. 5. GOES-II visible image of Felicia at 0000 UTC 6 Aug 2009, the time of the cyclone's peak intensity. Image courtesy of the U.S. Naval Research Laboratory's tropical cyclone webpage ([http://www.nrlmry.navy.mil/tc\\_pages/tc\\_home.html](http://www.nrlmry.navy.mil/tc_pages/tc_home.html)).

convection increased and became better organized, and a tropical depression formed around 1800 UTC 3 August. The depression became a tropical storm 6 h later while centered about 990 n mi southwest of the southern tip of Baja California.

In an environment of low vertical wind shear and over 28°–29°C waters, Felicia rapidly intensified and reached hurricane strength around 1800 UTC 4 August as it moved west-northwestward to the south of a deep-layer ridge. Felicia slowed its forward speed and turned northwestward on 5 August when it reached the western extent of the ridge and encountered a trough digging along 130°W. Although Felicia and Enrique came within 425 n mi of each other around 1200 UTC 6 August, their tracks indicate that there was little or no binary interaction between the two systems.

As Felicia turned northwestward, the cyclone continued to rapidly intensify and reached its estimated peak intensity of 125 kt at 0600 UTC 6 August while located about 1465 n mi east-southeast of Hilo, Hawaii (Fig. 5). Gradual weakening began during the next 24 h when Felicia moved over sea surface temperatures lower than 27°C. As new midlevel ridging built to the north and west of the hurricane, Felicia turned west-northwestward prior to crossing 140°W into the central North Pacific basin around 1200 UTC 8 August as an 80-kt hurricane.

The weakening trend continued on 9 August, when Felicia encountered rapidly increasing westerly vertical wind shear produced by a broad upper-level trough near

and north of the Hawaiian Islands. Aircraft reconnaissance indicated that the 700-hPa flight-level center became displaced from the surface center early on 9 August, and Felicia weakened to a tropical storm around 1200 UTC that day while centered about 550 n mi east of Hilo. Persistent shear caused the low-level circulation to become exposed around 0000 UTC 10 August, and Felicia's maximum winds diminished to 45 kt. Now a shallow cyclone, Felicia was steered westward for the remainder of its existence by a low- to midlevel subtropical ridge to its north.

Although weakening continued through 10 August, the upper-level trough responsible for the shear also created diffluence aloft, which helped to maintain an area of deep convection north-northeast of the low-level center. Aircraft reconnaissance and QuikSCAT data indicated that this convection supported winds of tropical storm force north of the circulation center through early the next day. Later that day deep convection diminished, and Felicia became a tropical depression by 1200 UTC 11 August while centered 120 n mi northeast of Hilo; the cyclone degenerated into a remnant low around 1800 UTC. The low-level circulation became ill defined and dissipated when it interacted with the high terrain of the Big Island of Hawaii.

While approaching the Hawaiian Islands, Felicia generated large swells that produced high surf of 6 to 10 ft (1.8 to 3.0 m) along east-facing shores during 10–12 August.

Widespread heavy rains and some freshwater flooding occurred as the remnants of Felicia passed through the islands from 11 to 13 August. The highest rainfall totals associated with the remnants of Felicia were 14.63 in. (372 mm) at Oahu Forest National Wildlife Refuge on Oahu, 13.46 in. (342 mm) at Mount Waialeale on Kauai, and 6.28 in. (160 mm) at West Wailuaki on Maui. The heavy rains caused the Waikane Stream to overflow its banks and sent floodwaters over the nearby road.

#### *g. Hurricane Guillermo, 12–20 August*

Guillermo was spawned by a large tropical wave that left the west coast of Africa on 26 July and entered the eastern North Pacific Ocean on 5 August. Convection associated with the wave increased on 8 August and an elongated surface low formed the next day. Deep convection increased markedly near the low center late on 11 August, and a tropical depression formed by 1200 UTC 12 August about 1380 n mi south-southwest of the southern tip of Baja California. The depression became a tropical storm 12 h later.

Guillermo intensified from a weak tropical storm into a major hurricane in about 48 h as it moved westward to west-northwestward. A banded eye was noted in visible satellite images late on 13 August, and Guillermo

became a hurricane early the next day. At that point, Guillermo's intensification was interrupted, but the banding eye structure developed into a central dense overcast. Rapid intensification resumed that afternoon, and Guillermo became a major hurricane on 15 August, reaching a peak intensity of 110 kt at 0600 UTC that day while located about 1220 n mi west of the southern tip of Baja California.

Guillermo began to weaken later that day when it moved over cooler waters, and the cyclone's intensity diminished to 65 kt when it crossed into the central Pacific basin very late on 16 August. Slow weakening continued during the next few days as the cyclone moved over cooler waters and encountered moderate westerly wind shear. By 0600 UTC 17 August, Guillermo weakened to a tropical storm while centered about 740 n mi east of Hilo. A QuikSCAT pass over the cyclone at 1648 UTC 17 August revealed winds of up to 45 kt within convection well removed from the exposed center. By 19 August, deep convection disappeared, and Guillermo degenerated into a remnant low while centered about 645 n mi north of Hilo.

As the low continued northwestward, it merged with a frontal zone and became extratropical near 1200 UTC 20 August about 700 n mi north of Hilo. The extratropical transition of an eastern Pacific tropical cyclone is a rare occurrence, with only two others noted in the observational record. At about the same time, deep convection reformed in the northeastern semicircle and QuikSCAT data indicated that maximum winds increased to 40 kt. The cyclone then turned northward, and convection began to weaken as the cyclone turned northeastward around 0600 UTC 21 August. Once again reduced to a swirl of low clouds, the low became elongated and was absorbed by a second cold front around 1200 UTC 23 August.

#### *h. Tropical Storm Hilda, 22–28 August*

Hilda was spawned by a tropical wave that exited the coast of Africa on 2 August and crossed Central America on 13 August. The wave moved westward over the eastern North Pacific Ocean for several days with few signs of development. By 18 August deep convection developed some organization, but it took three days for the system to develop a closed low-level circulation. Deep convection associated with the low organized further, and the system became a tropical depression around 1200 UTC 22 August, when centered 1140 n mi east-southeast of Hilo. Despite northeasterly vertical wind shear, the cyclone became a tropical storm 6 h later.

Hilda moved westward to the south of a subtropical ridge over the central North Pacific Ocean. Strengthening was limited by persistent northeasterly wind shear, and

Hilda crossed into the central North Pacific basin around 1200 UTC 23 August with an estimated intensity of 40 kt. Despite continuing moderate shear, Hilda intensified and reached its peak intensity of 55 kt around 0600 UTC 24 August, when it was located about 740 n mi south-east of Hilo. As Hilda moved slowly westward to the south of the same midlevel ridge for the next couple of days, the cyclone encountered an environment that was even less conducive thermodynamically. Weakening was slow at first but accelerated on 25 August when Hilda's convective structure deteriorated. The cyclone eventually weakened to a tropical depression by 0000 UTC 27 August while centered about 440 n mi south-southeast of Hilo. The depression produced persistent but limited convection for a short time as it continued westward but degenerated into a remnant low by 1800 UTC 28 August. The remnant circulation was steered west-northwestward by the low-level trade wind flow for the next three days before dissipating late on 31 August about 1090 n mi west-southwest of Hilo.

#### *i. Tropical Storm Ignacio, 24–27 August*

Ignacio formed from the same tropical wave that spawned Tropical Storm Ana in the Atlantic basin (Berg and Avila 2011). The southern portion of the wave entered the eastern North Pacific basin on 20 August, and convective activity began to gradually increase but remained disorganized. As the system moved west-northwestward, a broad area of low pressure formed on 22 August south of Cabo Corrientes, Mexico. By 1800 UTC 24 August, the system had enough organization to be classified as a tropical depression about 600 n mi southwest of the southern tip of Baja California, and the depression became a tropical storm 6 h later. Ignacio reached an estimated maximum intensity of 45 kt at 1200 UTC 25 August and maintained that intensity for about a day before weakening. The cyclone then turned northwestward and moved over cooler waters. It then degenerated into a remnant low at 1200 UTC 27 August and dissipated on 29 August.

#### *j. Hurricane Jimena, 28 August–4 September*

Jimena originated from a tropical wave that moved across the west coast of Africa on 15 August and reached the eastern North Pacific on 25 August. Associated convection increased in coverage on 27 August, and early the next day a low pressure area formed about 265 n mi southeast of Acapulco. A tropical depression then formed around 1800 UTC 28 August about 190 n mi south of Acapulco.

The cyclone strengthened very rapidly, becoming a tropical storm early on 29 August and a hurricane later

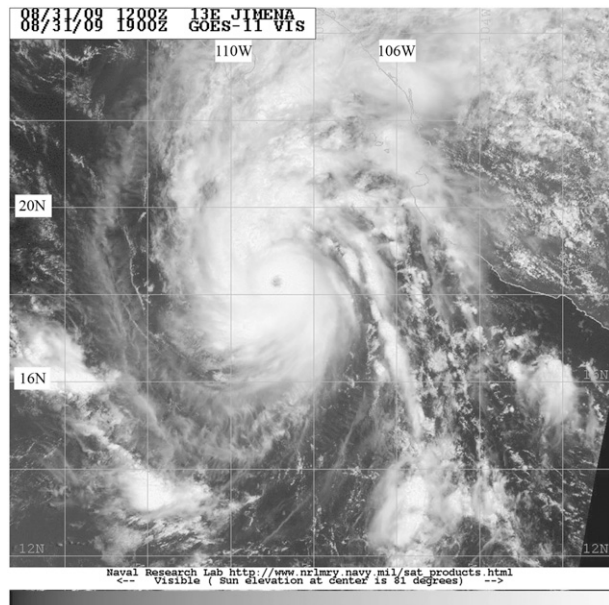


FIG. 6. GOES-11 visible image of Jimena at 1900 UTC 31 Aug 2009, near the time of the cyclone's peak intensity. Image courtesy of the U.S. Naval Research Laboratory's tropical cyclone webpage ([http://www.nrlmry.navy.mil/tc\\_pages/tc\\_home.html](http://www.nrlmry.navy.mil/tc_pages/tc_home.html)).

that day. Jimena initially moved westward on the south side of a midlevel ridge but turned northwestward on 30 August. Intensification continued until the hurricane reached an estimated intensity of 120 kt on 30 August. Development was then interrupted by an eyewall replacement cycle (e.g., Willoughby et al. 1982) that ended early on 31 August, and Jimena again began to intensify, reaching a peak intensity of 135 kt later that day (Fig. 6).

Late on 31 August, Jimena turned north-northwestward between the ridge to its east, Tropical Storm Kevin to the west, and a mid- to upper-level low west of Baja California. A combination of increasing vertical wind shear, cooler waters, and a second eyewall replacement cycle caused Jimena to weaken early on 1 September. Steady weakening and a north-northwestward motion continued until Jimena made landfall over Isla Santa Margarita, Baja California del Sur, around 1200 UTC 2 September with an estimated intensity of 90 kt (category 2 on the Saffir-Simpson Hurricane Wind Scale). After briefly moving into the adjacent Pacific waters, a second landfall occurred a few hours later at Puerto San Carlos, Baja California del Sur.

The center of Jimena reentered the Pacific before turning northward and making a third landfall east of San Juanico in Baja California del Sur, around 2100 UTC 2 September. Jimena then moved northward across Baja California while weakening to a tropical storm, and the center emerged into the central Gulf of California

TABLE 2. Selected surface observations for Hurricane Jimena, 28 Aug–4 Sep 2009.

Location	Min sea level pressure		Max surface wind speed			Storm surge (ft)	Storm tide (ft)	Tot rain (mm)
	Date/time (UTC)	Pressure (mb)	Date/time (UTC)*	Sustained (kt)	Gust (kt)			
Mexico								
International Civil Aviation Organization (ICAO) Sites								
MMGM–Guaymas, Sonora (27.97°N, 110.93°W)			03/1442	25	50			672
Automated stations								
Ciudad Constitucion (Baja Cal. del Sur)	02/1350	976.5	02/1340	61	79			333
San Juanico (Baja Cal. del Sur)	02/2030	988.1	02/2110	38	63			
San Lucas (Baja Cal. del Sur)			01/2350	49	60			
Socorro Island (Colima)	01/0800	997.5	01/0800	29	38			
Rainfall Stations								
Ciudad Obregon (Sonora)								76
Cocoraque (Sonora)								101
El Cajoncito (Baja Cal. del Sur)								94
Empalme (Sonora)								348
La Palmillita (Baja Cal. del Sur)								140
Loreto (Baja Cal. del Sur)								104
Navojoa (Sonora)								118
San Bartolo (Baja Cal. del Sur)								137
Santa Rosalia (Baja Cal. del Sur)								167
Public/Other								
La Paz (Costa Baja Resort)	02/0632	1006.1	02/1047		45			
Puerto San Carlos (Edds/Mongerman)	02/1310	973.0						

\* Date/time is for sustained wind when both sustained and gust are listed.

around 0600 UTC 3 September. The steering currents then collapsed, and Jimena drifted erratically over the Gulf for about 24 h and weakened to a tropical depression early on 4 September. The depression began moving southwestward later that day and made its final landfall near Santa Rosalia, Baja California del Sur, around 1900 UTC 4 September. As Jimena crossed Baja California, it degenerated into a remnant low and then dissipated over the Pacific on 5 September.

The 135-kt estimated maximum intensity of Jimena is based on a 700-hPa flight-level wind of 149 kt measured by a U.S. Air Force Reserve Hurricane Hunter aircraft at 1921 UTC 31 August and an SFMR surface wind estimate of 132 kt recorded a minute earlier. The minimum observed central pressure was 931 hPa at 1919 UTC that day. The central pressure was falling rapidly at that time, and the satellite signature of Jimena continued to become more impressive until around 2100 UTC. Therefore, the hurricane may have continued strengthening for a few hours after the aircraft departed.

Media reports indicate that Jimena's winds and rains caused widespread damage in central and southern Baja California, including the cities of Ciudad Constitución, Mulege, and Loreto, along with many smaller towns

near the track of the center. Severe freshwater floods occurred on the Mexican mainland near Guaymas in Sonora, where the maximum reported storm-total rainfall was 26.46 in. (672 mm). Ciudad Constitución in Baja California del Sur reported a sustained wind of 61 kt and a gust to 79 kt on 2 September, the highest wind report at any land station. While there were no observations of sustained hurricane-force winds, hurricane conditions likely affected much of the Pacific coast of Baja California south of San Juanico. Storm chasers in Puerto San Carlos reported a pressure of 973.0 hPa as the eye of Jimena passed over that town. Selected surface observations and other significant rainfall totals are included in Table 2.

Media reports indicated that the number of damaged buildings was in the tens of thousands; however, no monetary damage estimates are available. One death has been attributed to Jimena: a drowning due to freshwater flooding in Mulege, Baja California del Sur.

#### k. Tropical Storm Kevin, 29 August–1 September

Kevin originated from a tropical wave that entered the eastern North Pacific basin on 23 August. As the

wave moved westward, an area of low pressure formed along the wave on 27 August. Deep convection was intermittent before increasing early on 29 August, and it is estimated that a tropical depression formed around 1200 UTC that day, centered about 890 n mi southwest of the southern tip of Baja California. The cyclone moved west-northwestward and became a tropical storm at 1800 UTC 29 August, while centered about 910 n mi southwest of the southern tip of Baja California.

Kevin continued moving west-northwestward on the southeastern periphery of a mid- to upper-level subtropical ridge. At that point, a mid- to upper-level trough moving southwestward from Baja California and an anticyclone to Kevin's southeast induced a sharp northward turn late on 29 August. A general northward motion continued for the remainder of the cyclone's existence. Deep convection near the center of Kevin remained intermittent due to weak to moderate southeasterly vertical wind shear associated with the upper-level outflow of Hurricane Jimena, upper-level subsidence, and relatively dry air in the lower to middle troposphere. After reaching an estimated peak intensity of 45 kt from 0600 UTC 29 August, the cyclone began to slowly weaken while the convection decreased. Kevin became a tropical depression around 0600 UTC 31 August as it turned north-northwestward and northwestward. The depression degenerated into a remnant low around 1800 UTC, while centered about 730 n mi west-southwest of the southern tip of Baja California.

The remnant low of Kevin turned toward the northeast on 2 September and moved very slowly for a couple of days. The low then accelerated westward and then southwestward early 4 September prior to dissipating around 0600 UTC 6 September about 1200 n mi west-southwest of the southern tip of Baja California.

#### *l. Hurricane Linda, 7–11 September*

Linda developed from a tropical wave that moved across the west coast of Africa on 18 August. The northern portion of the wave developed into Tropical Storm Danny in the Atlantic basin east of the Bahamas on 26 August (Berg and Avila 2011), while the southern part continued to move westward and entered the eastern North Pacific basin on 28 August. Convective activity remained limited until 3 September, and an area of low pressure developed along the wave around 0000 UTC 6 September. Deep convection became organized enough for the low to be considered a tropical depression by 0600 UTC 7 September, while located about 980 n mi west-southwest of the southern tip of Baja California. The depression then strengthened to a tropical storm about 6 h later.

Linda moved very slowly westward over the next day or so as a subtropical ridge to its north weakened and

steering currents collapsed. Another midlevel ridge developed east of the cyclone by 9 September, and Linda accelerated northwestward. The storm gradually intensified during that time and became a hurricane by 1800 UTC 9 September, while centered about 1515 n mi west-southwest of the southern tip of Baja California. Linda reached an estimated peak intensity of 70 kt around 0000 UTC 10 September. Although a short-lived eye formed, vertical wind shear and cooler waters led to a quick degradation of the satellite presentation, and Linda weakened to a tropical storm by 0000 UTC 11 September. The cyclone degenerated into a remnant low by 0000 UTC 12 September once it lost all its deep convection, while centered about 1205 n mi west of the southern tip of Baja California. The remnant low moved generally southwestward for almost three days before dissipating about 1055 n mi east of Hilo.

#### *m. Tropical Storm Marty, 16–19 September*

Marty originated from a tropical wave that moved across the west coast of Africa on 28 August and entered the eastern North Pacific basin on 10 September. On 13 September disorganized convection developed in association with the wave and gradually increased in coverage. The convective activity slowly became better organized over the next day or two, and a broad area of low pressure formed along the wave around 1200 UTC 15 September. The system became a tropical depression while centered about 325 n mi south of the southern tip of Baja California.

The depression moved slowly northwestward on the western periphery of a midlevel subtropical ridge in an environment of moderate southeasterly wind shear. Despite the shear, which displaced the convection to the west of the circulation center, the cyclone slowly strengthened and became a tropical storm around 1200 UTC 16 September, when it was located 285 n mi south-southwest of the southern tip of Baja California. Weak steering currents caused Marty's forward speed to slow further, and the cyclone drifted northwestward to north-northwestward on 17 September without strengthening further. The cyclone then began to weaken when it encountered drier and more stable low-level air and increasing southwesterly wind shear associated with a mid- to upper-level trough located near Baja California. The weakening trend accelerated after Marty reached sub-27°C waters, and the cyclone weakened to a tropical depression around 1800 UTC 18 September about 285 n mi west-southwest of the southern tip of Baja California. Marty became a remnant low the following day after losing all deep convection. The remnant circulation moved west-northwestward for another three days before dissipating about 1200 n mi west of the southern tip of Baja California.

*n. Tropical Storm Nora, 23–25 September*

Nora originated from a tropical wave that entered the eastern North Pacific basin on 15 September. On 18 September, deep convection associated with the wave increased near the Gulf of Tehuantepec, and a low developed along the wave axis on 22 September. Late that day convection increased near the center of the low, and a tropical depression formed around 0000 UTC 23 September while centered about 560 n mi southwest of the southern tip of Baja California.

The depression strengthened into a tropical storm 6 h later as it moved west-northwestward to northwestward around the southwestern periphery of a midlevel subtropical ridge. In a favorable environment of low vertical wind shear and over warm waters, Nora strengthened over the next 18 h and reached a peak intensity of 50 kt around 0000 UTC 24 September, while centered about 600 n mi southwest of the southern tip of Baja California. However, cooler water and strong southwesterly wind shear associated with an upper-level trough then caused the cyclone to weaken while it turned westward under the influence of a low-level ridge to the north. Nora became a tropical depression around 0000 UTC 25 September about 710 n mi west-southwest of the southern tip of Baja California and degenerated into a remnant low 6 h later.

The remnant low persisted for about four days while moving west-southwestward to southwestward before it was absorbed into the intertropical convergence zone (ITCZ) about 1390 n mi west-southwest of the southern tip of Baja California.

*o. Tropical Storm Olaf, 1–3 October*

Olaf developed from a tropical wave that entered the western Caribbean on 23 September. The wave generated a large area of deep convection over this area as it interacted with an upper-level trough, and the convection remained active for several days before the wave moved into the eastern North Pacific on 24 September. An elongated low formed along the wave on 28 September a couple of hundred nautical miles southwest of Manzanillo and was close to becoming a tropical depression on 30 September. The associated deep convection briefly dissipated but returned that night in the northern portion of the large circulation, causing the center to reform to the north. A tropical depression developed around 1200 UTC October 1, when the system was located about 475 n mi west-southwest of the southern tip of Baja California.

Shortly after formation, the depression turned northward and became a tropical storm. Olaf continued moving northward around the western periphery of a midlevel ridge over northern Mexico and reached an estimated

peak intensity of about 40 kt around 1200 UTC 2 October. The system turned sharply eastward early the next day and weakened because of cooler waters and increasing southerly shear. Olaf weakened to a tropical depression at 0600 UTC 3 October and 12 h later degenerated into a remnant low about 135 n mi west-southwest of Cabo San Lázaro, Mexico. The remnant low slowed, turned east-northeastward, and moved onshore over the southern Baja California peninsula early the next day before dissipating.

Heavy rains associated with Olaf fell in portions of northwestern Mexico and southern Baja California, with the highest total of 5.22 in. (132.5 mm) reported in Carrizo, Sinaloa. Reports of flooding in the cities of La Paz and Comondú were received, but there were no reports of damage or casualties.

*p. Tropical Storm Patricia, 11–14 October*

Patricia formed from a tropical wave that emerged from the west coast of Africa on 23 September. This wave spawned Tropical Depression Eight in the Atlantic basin about 435 n mi west of the Cape Verde Islands on 25 September (Berg and Avila 2011) and continued westward, crossing Central America on 6 October. Widespread but sporadic deep convection was observed in association with the wave over the next few days, and a broad area of low pressure formed about 200 n mi south of Manzanillo on 9 October. On 11 October, convection persisted and a well-defined center of circulation developed, marking the formation of a tropical depression about 350 n mi south-southeast of the southern tip of Baja California.

The depression reached tropical storm intensity about 6 h after genesis while centered about 310 n mi south-southeast of the southern tip of Baja California. Patricia gradually strengthened over the next day while moving over very warm waters in an environment of light easterly vertical wind shear. While intensifying, the cyclone moved generally north-northwestward between a deep-layer ridge to its east and a mid- to upper-level trough to its northwest. Patricia reached its estimated peak intensity of 50 kt around 0000 UTC 13 October, while centered about 190 n mi south of the southern tip of Baja California.

The cyclone suddenly weakened on 13 October, possibly as a result of moderate southeasterly vertical wind shear and a more stable air mass. Deep convection dissipated late that day as the cyclone weakened further, and Patricia became a remnant low around 0600 UTC 14 October while centered just 25 n mi east-southeast of the southern tip of Baja California. The remnant low of Patricia then moved westward in the low-level trade winds for the next 36 h before dissipating.

### q. Hurricane Rick, 15–21 October

Rick originated from a tropical wave that moved across the west coast of Africa late on 3 October. A small low formed along the wave axis on 8 October a couple of hundred nautical miles east of the southern Windward Islands, but the low dissipated as it moved over northern South America from 9 to 11 October. The wave entered the eastern North Pacific basin on 12 October, and associated convection gradually increased in organization over the next few days while the wave moved westward south of Central America and the Gulf of Tehuantepec. A tropical depression formed within the wave around 1800 UTC 15 October, while centered about 300 n mi south-southwest of the Gulf of Tehuantepec.

Rick intensified to a tropical storm 6 h after formation and then rapidly intensified into a hurricane within 24 h as it moved west-northwestward, south of a deep-layer ridge. In an environment characterized by low vertical wind shear, high midlevel relative humidity, and sea surface temperatures near 30°C, rapid intensification continued for another 36 h. Rick attained major hurricane status by 1200 UTC 17 October and reached its estimated peak intensity of 155 kt around 0600 UTC 18 October (Fig. 7). Rick became the second-strongest hurricane ever recorded in the eastern North Pacific Ocean (since reliable records began in 1971; Blake et al. 2009), behind Hurricane Linda of 1997 (Lawrence 1999).

Rick then weakened almost as quickly as it strengthened due into strong southwesterly upper-level winds associated with an amplifying shortwave trough extending southward from the southwestern United States. Under the influence of the trough, the cyclone slowed and turned northwestward and then northward. Rick fell below major hurricane status by 1200 UTC 19 October and rapidly weakened to a tropical storm 18 h later, while centered about 235 n mi south-southwest of the southern tip of Baja California. Rick then accelerated while passing about 130 n mi south of the southern tip of the Baja peninsula late on 20 October and made landfall near Mazatlán, Mexico, around 1400 UTC 21 October with estimated maximum sustained winds of 50 kt. Sustained winds of 34 kt, a gust to 53 kt, and a minimum pressure of 989.9 hPa were reported at Mazatlán at 1226 UTC that day. Once inland, the tropical storm quickly dissipated as it moved over the rugged terrain of west-central Mexico and encountered strong southwesterly shear.

Media reports indicate that there were two deaths associated with large waves caused by Hurricane Rick. A 38-year-old man fishing from a rocky point was swept out to sea on 18 October at Los Cabos harbor, in San José del Cabo, and a 16-year-old boy drowned at El Medano Beach in Cabo San Lucas the following day.

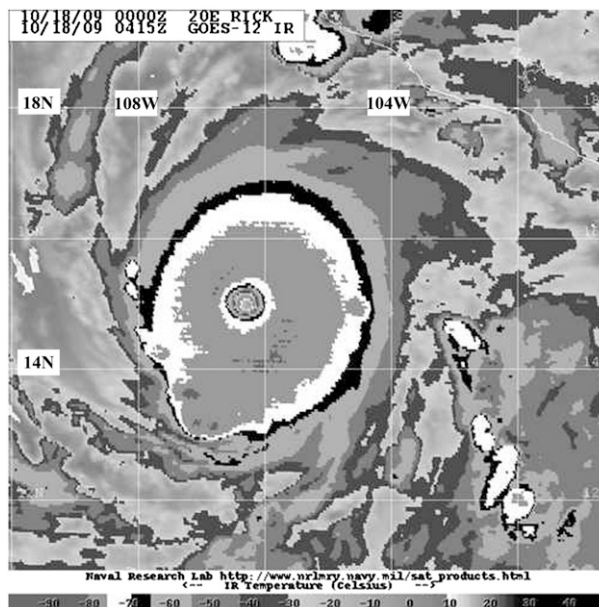


FIG. 7. GOES-12 infrared image of Rick with Dvorak enhancement curve (Dvorak 1984) at 0415 UTC 18 Oct 2009, at the time of the cyclone's peak intensity. Image courtesy of the U.S. Naval Research Laboratory's tropical cyclone webpage ([http://www.nrlmry.navy.mil/tc\\_pages/tc\\_home.html](http://www.nrlmry.navy.mil/tc_pages/tc_home.html)).

## 4. Tropical depressions

### a. Tropical Depression One-E, 18–19 June

Tropical Depression One-E can be traced to a tropical wave that entered the eastern North Pacific basin on 10 June with vigorous but disorganized convection. The wave moved westward, and a broad low formed late on 15 June several hundred miles to the south-southwest of Acapulco. The low moved west-northwestward on 16 June and then northwestward on 17 June while the low-level circulation became better defined. Convection increased near the low center early on 18 June, and a tropical depression formed around 1200 UTC that day, while centered about 350 n mi south-southwest of Mazatlán, Mexico.

The depression turned northward on 18 June and then turned north-northeastward the next day while it moved between the western periphery of a midlevel ridge over Mexico and an unusually deep upper-level trough approaching California. Although the depression was briefly close to tropical storm strength, the convection associated with the system began to weaken, and the low-level circulation became elongated by 19 June as it approached southwestern Mexico. The depression degenerated into an open trough of low pressure by 1800 UTC 19 June near Las Tres Marias, Mexico.

TABLE 3. Homogenous comparison of official (OFCL) and CLIPER5 track forecast errors in the eastern North Pacific basin for the 2009 season for all tropical cyclones. Averages for the previous 5-yr period are shown for comparison.

	Forecast period (h)						
	12	24	36	48	72	96	120
2009 mean OFCL error (n mi)	29.5	50.9	71.9	89.0	119.2	162.5	240.4
2009 mean CLIPER5 error (n mi)	38.4	76.6	119.8	165.4	248.1	306.3	352.2
2009 mean OFCL skill relative to CLIPER5 (%)	23.2	33.6	40.0	46.2	52.0	46.9	31.7
2009 mean OFCL bias vector ( $^{\circ}$ /n mi)	225/1	202/3	195/9	206/11	248/34	253/79	242/138
2009 No. of cases	236	204	173	143	99	69	45
2004–08 mean OFCL error (n mi)	31.0	51.7	71.7	90.2	123.6	161.3	201.8
2004–08 mean CLIPER5 error (n mi)	38.4	73.6	111.9	149.1	214.2	261.1	311.5
2004–08 mean OFCL skill relative to CLIPER5 (%)	19.3	29.8	35.9	39.5	42.3	38.2	35.2
2004–08 mean OFCL bias vector ( $^{\circ}$ /n mi)	314/3	298/5	289/9	288/15	272/16	271/7	006/7
2004–08 No. of cases	1299	1140	986	855	626	451	310
2009 OFCL error relative to 2004–08 mean (%)	–5	–2	0	–1	–4	1	19
2009 CLIPER5 error relative to 2004–08 mean (%)	0	4	7	11	16	17	13

*b. Tropical Depression Six-E (Lana),  
30 July–2 August*

Tropical Depression Six-E was the first eastern North Pacific tropical depression to later become a named storm in the central North Pacific basin since Hurricane Iniki in 1992. The tropical depression originated from a tropical wave that entered the eastern North Pacific basin on 21 July. The area of disturbed weather associated with the wave combined with another area of disturbed weather on 26 July, and by 0000 UTC 27 July the system was located between 115° and 120°W. As the system moved westward, vertical wind shear remained unfavorable for development for a couple of days. The shear decreased on 29 July, however, and a tropical depression formed around 1200 UTC 30 July about 1030 n mi east-southeast of Hilo. The depression moved quickly westward to the south of a subtropical ridge and crossed 140°W longitude into the central North Pacific basin where it became Tropical Storm Lana around 1800 UTC that day, while centered about 955 n mi east-southeast of Hilo.

Steady strengthening beneath upper-level anticyclonic flow continued for the next 24 h, and by 1800 UTC 31 July Lana reached its estimated peak intensity of 55 kt while located about 585 n mi southeast of Hilo. Increasing southwesterly vertical wind shear began to impinge upon Lana as it approached an upper-level trough over the Hawaiian Islands, and the cyclone gradually weakened during the next two days as it continued westward in the low- to midlevel flow to the south of a midlevel ridge. By 1800 UTC 2 August, Lana weakened to a tropical depression about 385 n mi south-southwest of Hilo. Thereafter, only small, intermittent bursts of convection appeared northeast of the center, and the system degenerated into a remnant low 6 h later. The low dissipated in the low-level trade wind flow shortly after 0600 UTC 3 August about 495 n mi southwest of Hilo.

*c. Tropical Depression Nine-E, 9–11 August*

Tropical Depression Nine-E formed from a tropical wave that entered the eastern North Pacific Ocean on 1 August. Satellite imagery indicated that the system remained poorly organized until 6 August, when a broad area of low pressure formed about 700 n mi south-southwest of the southern tip of Baja California. The circulation gradually became better defined over the next 24 to 36 h, although associated convection remained limited. Shortly before 1200 UTC 9 August, convection began to increase in association with the low, and a tropical depression formed by 1800 UTC (that day), about 770 n mi southwest of the southern tip of Baja California.

In an environment of moderate westerly wind shear, the depression did not strengthen as it moved generally westward during the next day or so. Although the depression was near tropical storm strength for a brief time, microwave imagery indicated that the low-level center was exposed to the west of the convective activity. Deep convection dissipated later that day, and the depression degenerated into a remnant low around 0000 UTC 12 August, while centered about 1200 n mi west-southwest of the southern tip of Baja California. The low moved west-southwestward during the next couple of days and was absorbed into the ITCZ shortly after 0000 UTC 15 August about 1825 n mi west-southwest of the southern tip of Baja California.

## 5. Forecast verification and warnings

For all operationally designated tropical cyclones in its area of responsibility, the NHC issues an official tropical cyclone track (latitude and longitude of the circulation center) and intensity (maximum 1-min wind speed at 10 m above the surface) forecast every 6 h. These forecasts are made for the 12-, 24-, 36-, 48-, 72-,

TABLE 4. Homogenous comparison of official (OFCL) and Decay-SHIFOR5 intensity forecast errors in the eastern North Pacific basin for the 2009 season for all tropical cyclones. Averages for the previous 5-yr period are shown for comparison.

	Forecast period (h)						
	12	24	36	48	72	96	120
2009 mean OFCL error (kt)	7.1	12.8	17.1	18.0	17.3	18.1	18.8
2009 mean Decay-SHIFOR5 error (kt)	8.0	13.6	17.9	20.8	19.7	17.6	16.0
2009 mean OFCL skill relative to Decay-SHIFOR5 (%)	11.3	5.9	4.5	13.5	12.2	-2.8	-17.5
2009 OFCL bias (kt)	-0.2	0.2	-0.4	-1.4	1.1	7.2	12.1
2009 No. of cases	236	204	173	143	99	69	45
2004-08 mean OFCL error (kt)	6.2	10.2	13.3	15.1	17.7	19.0	18.8
2004-08 mean Decay-SHIFOR5 error (kt)	7.1	11.5	14.7	16.8	18.9	20.3	20.2
2004-08 mean OFCL skill relative to Decay-SHIFOR5 (%)	12.7	11.3	9.5	10.1	6.3	6.4	6.9
2004-8 OFCL bias (kt)	0.9	2.2	3.2	3.0	3.7	2.0	-1.2
2004-08 No. of cases	1299	1140	986	855	626	451	310
2009 OFCL error relative to 2004-08 mean (%)	14.5	25.5	28.6	19.2	-2.3	-4.7	0.0
2009 Decay-SHIFOR5 error relative to 2004-08 mean (%)	12.7	18.3	21.8	23.8	4.2	-13.3	-20.8

96-, and 120-h periods from the initial synoptic time of the forecast (0000, 0600, 1200, or 1800 UTC). The forecasts are evaluated using the postseason 6-hourly best-track database for all tropical cyclones. The track error is defined as the great-circle distance between forecast and best-track positions of the tropical cyclone center, and the intensity error is the absolute value of the difference between the forecast and best-track intensities.

A comparison of the average track errors for 2009 and the previous 5-yr period for the official forecast and the CLIPER5<sup>4</sup> (Neumann 1972; Aberson 1998) model forecast are shown in Table 3, taken from Franklin (2010). CLIPER5 serves as a benchmark of track forecast skill. The 2009 NHC track errors (OFCL) were very close to the 5-yr means, except at 120 h where they were about 20% higher than the 5-yr mean. CLIPER5 errors, however, were somewhat above their long-term means, implying that forecasts were more difficult than average. Biases of the mean track forecasts were smaller than average though 48 h but significantly larger than average at 96 and 120 h; biases at the latter times were about 50% of the mean error magnitude and toward the west-southwest. Guillermo, which took a path more toward the northwest than expected, was a major contributor to these biases.

Table 4, also taken from Franklin (2010), compares official forecasts to the Decay-SHIFOR5 (see footnote 4) (Jarvinen and Neumann 1979; Knaff et al. 2003) model that serves as a benchmark for intensity forecast skill. Average official intensity errors (OFCL) were considerably above the 5-yr means through 48 h. However, Decay-SHIFOR5 forecast errors in 2009 were

above their 5-yr means by a comparable amount, suggesting that intensity forecasts were more difficult than average. Intensity forecast biases were small except at 96-120 h, where they were strongly positive. This is consistent with the pronounced southwestward bias of the track forecasts at these lead times as the storms were expected to remain over warmer waters longer than they actually did. However, the official forecast high bias at 96 and 120 h was higher than the bias in any of the guidance models, implying that the southwestward track bias cannot completely explain the bias in the official forecast.

*Acknowledgments.* The cyclone summaries are based on tropical cyclone reports written by the authors and Lixion Avila, Daniel Brown, Jack Beven, Richard Pasch, Eric Blake, Robbie Berg, John Cangialosi, and Chris Landsea of NHC. These reports are available online (at <http://www.nhc.noaa.gov/2009epac.shtml>). Portions of the summaries of cyclones that crossed 140°W into the central North Pacific basin were provided by Richard Knabb, Thomas Birchard, Derek Wroe, Sam Houston, and Jeffrey Powell of the Central Pacific Hurricane Center in Honolulu, Hawaii. Ethan Gibney of the I. M. Systems Group at the NOAA National Climatic Data provided the track maps.

#### REFERENCES

- Aberson, S. D., 1998: Five-day tropical cyclone track forecasts in the North Atlantic basin. *Wea. Forecasting*, **13**, 1005-1015.
- Bell, G. D., and Coauthors, 2000: Climate assessment for 1999. *Bull. Amer. Meteor. Soc.*, **81**, S1-S50.
- Berg, R. J., and L. A. Avila, 2011: Atlantic Hurricane season of 2009. *Mon. Wea. Rev.*, **139**, 1049-1069.
- Blake, E. S., E. J. Gibney, D. P. Brown, M. Mainelli, J. L. Franklin, and T. B. Kimberlain, 2009: Tropical cyclones of the eastern

<sup>4</sup> CLIPER5 and SHIFOR5 are 5-day versions of the original Climatology and Persistence (CLIPER) and Statistical Hurricane Intensity Forecast (SHIFOR) models.

- North Pacific basin, 1949–2006. Historical Climatology Series 6-5, National Climatic Data Center, 162 pp.
- Brennan, M. J., C. C. Hennon, and R. D. Knabb, 2009: The operational use of QuikSCAT ocean surface vector winds at the National Hurricane Center. *Wea. Forecasting*, **24**, 621–645.
- Brueske, K. F., and C. S. Velden, 2003: Satellite-based tropical cyclone intensity estimation using the NOAA-KLM series Advanced Microwave Sounding Unit (AMSU). *Mon. Wea. Rev.*, **131**, 687–697.
- Collins, J. M., 2007: The relationship of ENSO and relative humidity to interannual variations of hurricane frequency in the northeast Pacific Ocean. *Proc. 30th Applied Geography Conf.*, Indianapolis, IN, Association of American Geographers, 324–333. [Available online at <http://www.weathercenter.usf.edu/docs/research/jcollins/Collinspaper5.pdf>.]
- Demuth, J. L., M. DeMaria, and J. A. Knaff, 2006: Improvement of Advanced Microwave Sounding Unit tropical cyclone intensity and size estimation algorithms. *J. Appl. Meteor. Climatol.*, **45**, 1573–1581.
- Dvorak, V. F., 1984: Tropical cyclone intensity analysis using satellite data. NOAA Tech. Rep. NESDIS 11, 47 pp.
- Erickson, C. O., 1972: Evaluation of a technique for the analysis and forecasting of tropical cyclone intensities from satellite pictures. NOAA Tech. Memo. NESS 42, 28 pp.
- Franklin, J. L., cited 2010: 2009 National Hurricane Center Forecast Verification Report. [Available online at [http://www.nhc.noaa.gov/verification/pdfs/Verification\\_2009.pdf](http://www.nhc.noaa.gov/verification/pdfs/Verification_2009.pdf).]
- Hawkins, J. D., T. Lee, J. Turk, C. Sampson, J. Kent, and K. Richardson, 2001: Real-time internet distribution of satellite products for tropical cyclone reconnaissance. *Bull. Amer. Meteor. Soc.*, **82**, 567–578.
- Herndon, D., C. S. Velden, K. Brueske, R. Wacker, and B. Kabat, 2004: Upgrades to the UW-CIMSS AMSU-based TC intensity algorithm. *Extended Abstracts, 26th Conf. on Hurricanes and Tropical Meteorology*, Miami, FL, Amer. Meteor. Soc., 4D.1. [Available online at [http://ams.confex.com/ams/26HURR/techprogram/paper\\_75933.htm](http://ams.confex.com/ams/26HURR/techprogram/paper_75933.htm).]
- Jarvinen, B. R., and C. J. Neumann, 1979: Statistical forecasts of tropical cyclone intensity for the North Atlantic basin. NOAA Tech. Memo. NWS NHC-10, 22 pp.
- Kalnay, E., and Coauthors, 1996: The NCEP/NCAR 40-Year Reanalysis Project. *Bull. Amer. Meteor. Soc.*, **77**, 437–471.
- Knaff, J. A., M. DeMaria, B. Sampson, and J. M. Gross, 2003: Statistical, 5-day tropical cyclone intensity forecasts derived from climatology and persistence. *Wea. Forecasting*, **18**, 80–92.
- Lawrence, M. B., 1999: Eastern North Pacific hurricane season of 1997. *Mon. Wea. Rev.*, **127**, 2440–2454.
- Neumann, C. B., 1972: An alternate to the HURRAN (hurricane analog) tropical cyclone forecast system. NOAA Tech. Memo. NWS SR-62, 24 pp.
- Olander, T. L., and C. S. Velden, 2007: The advanced Dvorak technique: Continued development of an objective scheme to estimate tropical cyclone intensity using geostationary infrared satellite imagery. *Wea. Forecasting*, **22**, 287–298.
- Rappaport, E. N., and Coauthors, 2009: Advances and challenges at the National Hurricane Center. *Wea. Forecasting*, **24**, 395–419.
- Saffir, H. S., 1973: Hurricane wind and storm surge. *Mil. Eng.*, **423**, 4–5.
- Schott, T., and Coauthors, 2010: The Saffir–Simpson hurricane wind scale. National Weather Service. [Available online at <http://www.nhc.noaa.gov/pdf/sshws.pdf>.]
- Simpson, R. H., 1974: The hurricane disaster potential scale. *Weatherwise*, **27**, 169 and 186.
- Ulhorn, E. W., and P. G. Black, 2003: Verification of remotely sensed sea surface winds in hurricanes. *J. Atmos. Oceanic Technol.*, **20**, 99–116.
- Velden, C., and Coauthors, 2006: The Dvorak tropical cyclone intensity estimation technique: A satellite-based method that has endured for over 30 years. *Bull. Amer. Meteor. Soc.*, **87**, 1195–1210.
- Willoughby, H., J. Clos, and M. Shoreibah, 1982: Concentric eye walls, secondary wind maxima, and the evolution of the hurricane vortex. *J. Atmos. Sci.*, **39**, 395–411.

Copyright of Monthly Weather Review is the property of American Meteorological Society and its content may not be copied or emailed to multiple sites or posted to a listserv without the copyright holder's express written permission. However, users may print, download, or email articles for individual use.